Y/DZ-2160

Y-12

OAK RIDGE
Y-12
PLANT

LOCKHEED MARTIN

Novel Computational Simulation of Redox Reactions Within a Metal Electrospray Emitter

Gary J. Van Berkel
Jonathan S. Bullock, IV
Gary E. Giles
Leonard J. Gray

Issue Date: January 13, 1999

MANAGED BY
LOCKHEED MARTIN ENERGY SYSTEMS, INC.
FOR THE UNITED STATES
DEPARTMENT OF ENERGY

UCN-13672 (26 6-95)

DISCLAIMER

Novel Computational Simulation of Redox Reactions within a Metal Electrospray Emitter

Gary J. Van Berkel,[*1] Gary E. Giles,[*2] Jonathan S. Bullock, IV[*3], and Leonard J. Gray[*4]

[1]Chemical and Analytical Sciences Division, Oak Ridge National Laboratory, Oak Ridge, TN 37831-6365

[2]Computational Physics & Engineering Division, Oak Ridge National Laboratory, Oak Ridge, TN 37831-6415

[3]Development Division, Oak RidgeY-12 Plant, Oak Ridge, TN 37831-8096

[4]Computer Science and Mathematics Division, Oak Ridge National Laboratory, Oak Ridge, TN 37831-6367

Submitted to
Journal of the American Chemical Society

*To whom correspondence should be addressed

email:	vanberkelgj@ornl.gov	geg@ornl.gov	jsb@ornl.gov
phone:	423-574-1922	423-574-8667	423-574-1735
fax:	423-576-8559	423-576-0003	423-576-6986

ABSTRACT

To further both our fundamental understanding and our understanding of the analytical implications of the electrolytic nature of the electrospray ion source, in the context of electrospray mass spectrometry (ES-MS), a computational simulation of the oxidation of chemical species inside a metal emitter has been developed. The analysis code employs a boundary integral method for the solution of the Laplace equation for the electric potential and current, and incorporates standard activation and concentration polarization functions for the redox active species in the system to define the boundary conditions. The specific system modeled consisted of a 100 μm-i.d., inert metal capillary ES emitter and a spray solution comprised of an analyte dissolved in CH_3CN/H_2O (90/10 v/v). Variable parameters included the concentration (i.e., 5, 10, 20, and 50 μM) of the easily oxidized analyte ferrocene (Fc, dicyclopentadienyl iron) in the solution, and solution conductivities of 1.9, 3.8, and 7.6×10^{-7} Mho/cm. ES currents were on the order of 0.05 μA and the flow rate was 5 μL/min. Under these defined conditions, the two most prominent reactions at the emitter metal/solution interface were assumed to be H_2O oxidation ($2H_2O = O_2 + 4H^+ + 4e^-$) and Fc oxidation ($Fc = Fc^+ + e^-$). Using this model it was possible to predict the interfacial potentials, as well as the current density for each of the reactions, as a function of axial position from the emitter spray tip back upstream, under the various operational conditions. Computational fluid dynamics (CFD) calculations showed that the imposed flow rate through the emitter was adequate to prevent significant back-diffusion of Fc^+ into the emitter against the flow direction. The computational simulations predict the same behavior for the ES ion source as has been observed experimentally and is consistent with the controlled-current electrolytic cell analogy of Van Berkel and Zhou (Anal. Chem. **1995**, **67**, 2916-2923). Furthermore, the simulations demonstrate that the majority of the current involved in the redox reactions originated within a 200-300 μm region near the spray tip.

INTRODUCTION

The electrospray (ES) ion source is used to generate gas-phase ions from analyte species originally in solution, for interrogation and detection by mass spectrometry (MS). The ES-MS combination has literally revolutionized the field of mass spectrometry, permitting the analysis of a wide variety of analytes heretofore difficult or impossible to analyze. Electrospray has also provided a facile means of coupling condensed-phase separation methods on-line with MS. Applications of ES-MS span a broad range of categories, from simple molecular weight and structure determinations to complex studies of the solution chemistries and gas-phase structures of biopolymers (see e.g., refs. 1 and 2). Despite the widespread utility of ES-MS, fundamental studies aimed at elucidating the individual steps in the ES process responsible for the liberation of gas-phase ions from the solution are as yet incomplete. One would hope to develop from such fundamental studies a complete understanding of the overall process to take the guesswork out of optimizing parameters for analysis of a particular analyte. Furthermore, such understanding would surely lead to new and better analytical and fundamental applications of ES-MS. Our interest lies in obtaining a fundamental understanding of the electrolytic nature of the ES ion source and in understanding the analytical implications of this process as it relates to the practice of ES-MS.[3-5]

An Overview of Electrospray. The most common ES ion source configuration, as shown in Figure 1a, is comprised of two electrodes, viz., a narrow bore metal ES capillary or emitter (i.e., the working electrode) held at a high positive voltage (positive ion mode) or negative voltage (negative ion mode) and the atmospheric sampling aperture plate (i.e., the counter electrode) of the mass spectrometer held at a voltage at or near ground. Under typical ES-MS operating conditions, a solution containing the analyte of interest (which is normally ionic) is pumped through the ES emitter, and sprayed towards the aperture plate. Addition of any ionic species (i.e., electrolytes) to the solution, other than the analyte (or small amounts of acids or bases to ionize the analyte), is usually avoided when possible, as their presence in solution tends to suppress the formation of gas-phase ions from the analytes of interest.[6,7] However, some number of ions, either the analytes, contaminants, or deliberately added electrolytes, must be present in the solution or the ES device will not form charged droplets.[8] This is because electrophoretic charge separation of these

ions in solution is responsible for both formation and charging of the ES droplets. Under the influence of the applied electric field, ions of the same polarity as the voltage applied to the ES capillary migrate from the bulk liquid towards the liquid at the capillary tip, while ions of the opposite polarity migrate in the opposite direction back into the capillary. When the buildup of an excess of ions of one polarity at the surface of the liquid reaches the point that coulombic forces (as a result of the electric field between the liquid surface and the counter electrode) are sufficient to overcome the surface tension of the liquid, droplets enriched in one ion polarity are emitted from the capillary. This condition results in a quasi-continuous steady-state current at the counter electrode[9] with a direction consistent with the polarity of the voltage applied to the capillary.

For this continuous loss of one ion polarity in the charged-droplets to be sustained, the buildup of opposite charge in the capillary must be neutralized to maintain charge balance. As we presently understand it,[3-5] this charge-balancing process involves electrochemical oxidation/reduction of the components of the metal ES emitter and/or one or more of the species in the solution, ultimately leading to electron flow to or from the high voltage supply depending on the polarity applied to the capillary. Specifically, oxidation reactions occur in the ES emitter in positive ion mode, while reduction reactions occur in negative ion mode. The current that can be measured at the emitter owing to these reactions (i.e., the faradaic current) is equal in magnitude to the current measured at the counter electrode (i.e., the ES current), but of the opposite polarity (i.e., this is a series circuit). These reactions discharge excess ions and/or create ions of the appropriate polarity, thereby neutralizing the excess charge. Reduction/oxidation of some species at the counter electrode occurs to complete the electrical circuit.

On the basis of the operational configuration and the results of experimental study, Van Berkel and Zhou[4] concluded that the ES ion source operates electrolytically in a fashion analogous to a two-electrode controlled- or constant-current (CCE) flow cell.[10,11] The ES ion source, like a conventional CCE cell, is a two electrode cell (Figure 1a) and the charged droplet formation process may be viewed as the rate-controlling process. The cell current, i.e., the ES current, is determined by the product (charged droplet formation rate) $\times$ (average number of charges per

droplet). Altering the output of this current source requires that the rate of droplet production and/or the average number of charges per droplet be altered. As expressed by the modified Hendricks equation,[12-14] this may be accomplished by changing one or more of several operational parameters, including the dielectric constant and surface tension of the solvent, the volumetric flow rate through the ES capillary, the specific conductivity of the solution, and the imposed electric field at the capillary tip. In direct analogy to two-electrode controlled-current electrolysis, the potential distribution within the ES emitter (which ultimately determines which redox reactions can occur) is expected to be, for a given magnitude of ES current, that necessary to oxidize/reduce species in the solution at a rate sufficient to maintain that current. As such, the interfacial potential distribution and the redox reactions that take place in the emitter are expected to be a complex function of a number of factors including: (i) the ES current (and the factors which affect current); (ii) the working electrode material and effective area; (iii) the relative redox potential and concentration of the various electroactive species present; and (iv) the solution flow rate. It should be kept in mind that 96-97% of the voltage in this system is dropped across the gas (atmosphere) gap between the emitter and the counter electrode; thus, change in the ES conditions within the capillary tend to be overshadowed with respect to the overall resistance, and thus approximate constant-current conditions are obtained by default for a given solution conductivity. Unfortunately, it is not at this time feasible to experimentally measure the potential distribution within the ES emitter, nor can all the possible redox products be easily detected or quantified. Detection of these products by ES-MS requires that they readily form gas-phase ions; or in the ES-photodiode array system used by Van Berkel and coworkers,[4,15-17] that they cause a change in the UV/visible spectrum of the solution exiting the emitter.

Computational Simulation of the ES Electrolytic Process. This paper presents a computational simulation of the oxidation of chemical species inside an inert metal (e.g., platinum) ES emitter capillary in a positive ion mode ES-MS. The goal of this work was to develop methods to calculate the interface potential and current density distribution along the length of the emitter, for each of the possible redox reactions under the various operational conditions. It is expected that the modeling results can be used to begin to evaluate the degree of control possible over the redox reactions that take place in the ES[4] emitter. The ability to control, or at least know, the potentials and which redox reactions occur under various operational parameters might be exploited for analytical purposes in ES-MS.[5,15,16,18,19]

Governing Equations. This model of the electrochemical system in the ES emitter assumes that diffusion, convection, and migration of ions can be approximated by firstly solving the Laplace equation for the potential through the electrolyte volume, and its interaction with the electrolyte conductivity, to produce a current density distribution. The numerical solution thus obtained for the current density distribution is then modified by the nonlinear boundary conditions at the electroactive surfaces (electrodes). These boundary conditions approximate the effects of electrochemical surface reactions (activation polarization) and of mass-transfer effects (concentration polarization).[20-22]

Constant electrical conductivity is assumed throughout the electrolyte. This assumption places all the nonlinearities on the boundaries.

The oxidation of species at the metal-solution interface of the ES emitter is described by Faraday's law. The oxidation rate Ω (equivalents/s-cm^2) for an ideal single reaction system is proportional to the current density I (A/cm^2) at the emitter (i.e., anode) surface,

$$\Omega = \frac{\varepsilon}{nF}|I|, \qquad (1)$$

where F is Faraday's constant, ε is the current efficiency of the process, and n is the number of electrons involved in the reaction. The current density on the anode is in turn proportional to the normal derivative of the potential $\phi(x,y,z)$,

$$I = k\nabla\phi \cdot \tilde{n} \equiv k\frac{\partial\phi}{\partial\tilde{n}}, \tag{2}$$

where $\tilde{n}$ is the surface (unit) normal vector and k is the conductivity of the electrolyte (Mho/cm). The potential field ϕ satisfies the Laplace equation

$$\nabla^2\phi = 0 \ . \tag{3}$$

Thus, the current density is obtained by solving eq 3 subject to specified boundary conditions. The boundary of the region (Σ) consists of: (i) insulated surfaces, for which the applied boundary condition is zero normal flux ($\partial\phi/\partial\tilde{n} = 0$); and (ii) potential surfaces (anode and cathode). Using Green's Theorem, it can be shown that the Laplace equation is equivalent to the boundary integral equation

$$\phi(P) + \iint_{\Sigma} \frac{\partial G(P,Q)}{\partial\tilde{n}}\,\phi(Q)dQ = \iint_{\Sigma} G(P,Q)\,\frac{\partial\phi(Q)}{\partial\tilde{n}}\,dQ \tag{4}$$

where the Green's function is the point source potential

$$G(P,Q) = \frac{1}{4\pi\|P-Q\|} \ . \tag{5}$$

Here, the gradient and the surface integration are with respect to the boundary point Q, P is an arbitrary point on the boundary Σ, and $\|P-Q\|$ is the distance between P and Q. Equation 4 provides, for each P, a linear relationship between the values of ϕ and the gradient of ϕ on the boundary, and is the starting point for the Boundary Element Method solution of eq 3.

The boundary condition on the anode is not simply the applied potential; it must also take into account the nonlinear transfer (polarization) function describing the physical phenomena occurring in the boundary layer near the surface. In this work a virtual cathode is used to replace the jet structure, the spray plume, and the space between emitter and the counter electrode, and thus it completes the electrochemical cell (Figure 1b). The virtual cathode represents a surface of constant potential and is used to limit the model to the region where the governing equations are

directly applicable. Since the virtual cathode represents an isopotential surface in space no electrochemical reactions occur on this surface. Thus, the overvoltage and equilibrium voltage for the cathode are not applicable and are replaced by a constant V_C.

The polarization function on the anode specifies a nonlinear relationship between the current and the potential difference across this layer, and thus the entire problem is nonlinear. More specifically, if V_A and V_C denote the applied anode and cathode potentials ($V_A \geq V_C$), the applied voltage difference $V = V_A - V_C$ can be decomposed as a potential drop in the electrolyte, ΔV_{ir}, plus interfacial potential drops across the electrolyte boundary layers, made up of the overvoltages η together with their associated equilibrium potential values E^0 (Eq. 6). This is schematically illustrated in Figure 2 for a system involving two reactions.

$$V = (E^0 + \eta_T) + \Delta V_{ir} - V_C \qquad (6)$$

In general, the polarization is specified by the solution of the nonlinear relationship between the local current density and the overvoltage,

$$I = \mathsf{F}(\eta) \qquad (7)$$

The unknown overvoltage, together with the equilibrium potential for each reaction at the anode and the virtual cathode voltage, define the electrode boundary conditions for the Laplace equation, and must be determined self-consistently with eqs. 3, 6, and 7. In this work, the total anode overvoltage, η_T is comprised of two components, one part due to the effects of electron transfer (activation polarization) η_a, and the other due to the effects of mass transfer (concentration polarization) η_c :

$$\eta_T = \eta_a + \eta_c \ . \qquad (8)$$

(Other resistance effects at the interface, which would have different transfer functions, are ignored.) For activation polarization, the current/voltage relationship is given by the Butler-Volmer equation,

$$I = I_0\left(e^{\frac{\alpha_A F}{RT}\eta_a} - e^{-\frac{\alpha_C F}{RT}\eta_C} \right), \qquad (9)$$

while the functional form of the concentration polarization is

$$\eta_c = \frac{RT}{nF}\ln(1 - \frac{I}{I_L}) \quad . \qquad (10)$$

In these equations R is the gas constant, T is the temperature in Kelvin, α_A and α_C are the anodic and cathodic transfer coefficients, and I_0 is the exchange current. The α_A, α_C, and I_0 are the parameters that control the activation polarization. I_0 is the value of either anodic or cathodic current (at equilibrium, where these two currents are equal and opposite) associated with zero activation overvoltage ($\eta_a = 0$). Since at zero activation overvoltage the external currents are zero, I_0 must be determined indirectly by extrapolation on a current versus voltage plot. The transfer coefficients α_A and α_C are in general different and essentially define, with I_0, the rate constants for the cathodic and anodic reactions at the electrodes. All of these parameters are dependent on the specific electrode reactions, electrolyte composition, etc., and are experimentally determined. The limiting current density, I_l, is the primary variable controlling the concentration polarization. In this model the sum of all current at a location is controlled by the rate of transfer of electroactive species to or from the surface across the concentration boundary layer. All potentials/voltages are with respect to the standard hydrogen electrode (SHE) at 0.0 V.

The concentration boundary layer (illustrated in Figure 3) is defined as the region near the electrode through which mass transport perpendicular to the surface occurs only by diffusion (also called the diffusion boundary layer, δ). The outer boundary of this layer is determined by the point at which the concentration of the reacting species is equal to the bulk concentration. This position is generally determined by a linear extrapolation of the near-surface concentration gradient to the bulk concentration. The diffusion layer for most electrolyte systems is thinner than the hydrodynamic (momentum) boundary layer. This condition is a consequence of the relative effectiveness of mass transport by diffusion or viscous forces. Electrochemical reactions at the surface will decrease the

concentration of reacting species near the surface. The limiting current for a reaction is reached when the reacting species have been depleted from δ and only the molecules that diffuse across δ will reach the surface. The diffusion coefficient will thus limit the amount of the species that can react at the surface.

(i) Polarization Model for Multiple Reactions. There is the possibility of multiple reactions occurring simultaneously within the ES emitter. For the purposes of simplicity in this initial study, all reactions were assumed to be anodic and thus contribute an algebraically positive portion of the total current, which is the sum of the currents for each reaction. Also for simplicity, ES conditions were chosen such that only two reactions could be assumed to take place (see below). Multiple reactions were modeled as parallel electrical (ion) paths at the surface with separate activation (eq 9) and concentration (eq 10) polarization and separate equilibrium potentials as shown in Figure 2.

For a given location, the voltage on the electrolyte side of the polarization region, i.e., the interface potential V_{0A} in Figure 2, is assumed to be the same regardless of the reaction. The equilibrium potential and polarization components for each reaction ($E^0 + \eta_a + \eta_c$) must sum to V_{0A} at this point. The total current from V_{0A} to V_A is the sum of the currents of the individual reaction components. A solution is found when these conditions are satisfied.

(ii) The Specific ES System Modeled. The model was developed for an ES ion source of the basic geometry shown in Figure 1a with a 100 μm-i.d. inert metal ES emitter held at a positive 3.5 kV relative to a counter electrode at ground, spaced 1.0 cm away. The solvent/electrolyte system was CH_3CN/H_2O (90/10 v/v) containing various concentrations of ferrocene (Fc, dicyclopentadienyl iron). The most prominent redox reactions within the emitter under these conditions were assumed to be H_2O oxidation (eq 11) and Fc oxidation (eq 12).

$$\mathbf{2H_2O = O_2 + 4H^+ + 4e^-,} \qquad \mathbf{(11)}$$

$$\mathbf{Fc = Fc^+ + e^-,} \qquad \mathbf{(12)}$$

The electrochemical parameters governing these reactions are listed in Table 1 and represent the best values that we could extract from literature sources. The α_a for H_2O oxidation was estimated from eq 13.[23]

$$\alpha_a = \frac{(2.303RT)}{bF} \tag{13}$$

where b = v/decade from a polarization plot of log(current) versus potential(value = 0.12 for oxygen).[24] The α_a for Fc oxidation was assigned the same value. The equilibrium potential for Fc/Fc^+ was taken from Kuwana, et al.[25] The exchange current densities, I_0 ,were estimated from data tabulated by Newman[23] and Hampel.[26] The limiting current density was calculated using eq 14,[27]

$$I_l = -DnFC / \delta \tag{14}$$

where D is the diffusion coefficient, C is the bulk concentration, and δ is the diffusion boundary layer thickness (assumed 2×10^{-3} cm). The conductivity of CH_3CN/H_2O (90/10 v/v) was obtained from Janz and Tomkins.[28]

Detailed in Figure 1b, the electrolyte solution was modeled as extending from the end of the emitter into a truncated "Taylor cone" (a 49.3° cone)[29] which forms due to the balance between the electrical field forces and the surface tension of the liquid. The radial surface of this frustum was modeled as an insulator because ion flow is restricted to the axial direction (toward the end of the frustum). The cylindrical outer surface of the electrolyte inside the tube contacts the inner surface of the metal emitter and thus it was modeled as a potential surface. The upstream end of the electrolyte within the emitter was modeled as a flat insulated disk to truncate the model for computational efficiency.

The products of the redox reactions within the ES emitter travel from the inner emitter wall through the tube, into the Taylor cone, out the jet, and into charged droplets. In our simulation, the locus of current transfer into the jet is modeled as a flat-disk virtual cathode (with polarization defined as zero). The virtual cathode, as shown in Figure 1b, is placed on the truncated end of the

Taylor cone. The diameter of this virtual cathode was estimated from the size of the jet (or initial droplets) using a number of reasonable assumptions (see APPENDIX for details). The voltage difference, V, between the emitter (anode) and the virtual cathode was fixed in the BEPLATE code simulation at 130 V. This value, when used in the model, produced the same ES current (i.e., 5.21×10^{-8} A) as that experimentally measured at a solution flow of 5.0 μL/min using the ES geometry and solvent composition described above. Note that this voltage drop is consistent with that calculated by Juhasz et al.[13]

RESULTS

The solvent system for the initial ES system model was comprised of CH_3CN/H_2O (90/10 v/v) containing 5.0 μM Fc. The predicted interface potential distribution (V_{0A}) and the current densities (A/cm^2) for both H_2O and Fc oxidation, are plotted in Figure 4 as a function of axial position along the inner surface of the ES capillary. V_{0A} includes the effects of the equilibrium potentials and of activation and concentration polarizations for both reactions (Figure 2). The plot in Figure 4a covers from the spray tip of the emitter (0 μm) up to 1000 μm upstream, while the plot in Figure 4b shows just the 250 μm region at the tip. As one moves from the upstream portion of emitter to the spray tip, the total current density gradually increases, but goes through a rather complicated transition near the tip. This is due to the relative electrochemical parameters of the two competing, parallel redox processes taking place within the emitter. In the low current density region, far from the tip, Fc oxidation supplies the majority of the current. As one approaches the tip, the rate of this reaction increases to a point limited by the maximum achievable flux of material to the electrode, i.e., the limiting current, I_l. At this point, the potential at the electrode surface is such that the Fc reacts as fast as it reaches the surface. An increase of V_{0A} beyond this value cannot increase the rate for this reaction. To supply more current, the interfacial potential increases, which increases the rate of H_2O oxidation. Therefore, both the interface potential and current owing to H_2O oxidation are observed to increase substantially at about the same point as which the limiting current for the Fc reaction is reached. The current due to H_2O oxidation continues to increase as one travels downstream.

Figure 5 shows data from the same set used to create Figure 4, presented as log(current density) versus interface potential. This is the plotting convention typically used to illustrate electrochemical reaction kinetics and is the same convention used to determine the parameter ***b*** of eq 13. Plotted in this way, the calculated results for this system appear quite reasonable. The Fc reaction does not begin until the interface potential is more positive than its equilibrium potential of +0.572 V. The straight-line section of this plot has the correct slope (0.12 V/decade), and the plot makes a transition to an asymptote of 6×10^{-6} A/cm^2 as it should due to concentration polarization (limiting current) effects (from eq 14). The H_2O oxidation process plot is similarly consistent with its input parameters. The sum of the two partial reactions (which is the externally-measured current) makes a smooth transition from Fc oxidation as the dominant reaction to H_2O oxidation as the dominant reaction.

The calculated interface potential distributions and the integrated currents for both H_2O and Fc oxidation (normalized relative to the total ES current) as a function of axial position along the emitter, for four different concentrations of Fc, are plotted in Figure 6. This includes data for 5.0 μM of Fc already shown in Figure 5. These data reveal several important trends. First, as the concentration of Fc is increased, the interface potential plots, while maintaining the same basic shape, are shifted towards the emitter tip (Figure 6a). That is, the interface potential along the majority of the emitter length decreases as the concentration of Fc increases. Second, the majority of the current owing to either redox reaction is due to reactions that take place within 200 μm of the spray tip (Figure 6b). In fact, more than 95% of the oxygen is generated within 50 μm of the tip. And third, as the concentration of Fc is increased, the fraction of the total current supplied by Fc oxidation increases while that supplied by H_2O oxidation decreases (Figure 6b). In fact, at 50 μM Fc about 35% of the current is supplied by Fc oxidation. The data in Table 2 were extracted from the data in Figure 6b and show that, although the fraction of the total current owing to Fc oxidation increases with Fc concentration, the fraction of the Fc that travels through the emitter that is oxidized decreases. Thus, the "electrolysis efficiency" for Fc oxidation decreases with increasing Fc concentration. Note that the effect of varying the concentration of Fc was investigated by

scaling the electrochemical parameters with a linear dependence on concentration. Linear dependence is an approximate compensation model, but is a relationship appropriate for this level of simulation.

The calculated interface potential distributions and the integrated currents for both H_2O and Fc oxidation (normalized relative to the total ES current) as a function of axial position along the emitter, for three different solution conductivities (but a constant [Fc] = 5.0 μM) are plotted in Figure 7. These data include those from Figure 4 for a solution conductivity of 3.8×10^{-7} Mho/cm and additional data for a conductivity 2 times lower and also 2 times higher than this nominal value. One observes from Table 3 that as the conductivity of the solution is increased, the calculated total current increases. Since a condition of this model is a constant 130 V cell potential ($V_A - V_C$ in Figure 2), this is to be expected as discussed earlier regarding the aspects of the model compared with constant-current operating conditions. The interface potential increases all along the length of the emitter as conductivity increases (Figure 7a) and the fractional current (with respect to total current) from H_2O oxidation increases in a manner consistent with this increase in interface potential (Figure 7b). Also as the conductivity increases, the fractional current due to the ferrocene oxidation decreases. In this case, Fc oxidation supplies only about 13% of the total current at the highest solution conductivity. However, the data in Table 3 which were extracted from this plot confirm that the "electrolysis efficiency" for Fc oxidation increases with increasing conductivity. About 15% of the Fc flowing through the emitter is oxidized at a conductivity of 7.6×10^{-7} Mho/cm whereas approximately 8% is oxidized at a conductivity of 1.9×10^{-7} Mho/cm.

DISCUSSION

The results presented here represent the first computational simulation of the electrochemical operation of the ES ion source. This was accomplished through adaptatation of the BEPLATE™ code, originally developed for large-scale electroforming simulations,[20] to operate at the small scale of the ES emitter and to handle multiple, competitive redox reactions. Although the simulations were computationally intensive, converged solutions were achieved. These provided

predictions of the interface potential and of the separate current densities due to each of two reactions, as a function of axial position along the emitter inner surface. The most challenging aspect of the simulations involved solving the non-linear, multiple-reaction, polarization equations. The present algorithm employed a modified Picard (successive substitution) iteration.[30] To achieve convergence, a small underrelaxation factor (i.e., 1.0×10^{-6} - equivalent to a high "damping" factor) was required; although acceleration techniques were used, the calculations were very time consuming and sometimes failed to reliably converge. Work towards an improved non-linear solution method dealing directly with the nonlinearity of the polarization functions is in progress.

From this initial modeling of the electrolytic nature of ES, two major pieces of information were obtained. First, the computational simulations predicted basically the same electrolytic behavior for the ES ion source as has been observed experimentally[5] and is consistent with the controlled-current electrolytic cell analogy put forward by Van Berkel and Zhou.[4] That is, the situation within the ES emitter is not one of controlled-electrode-potential. Instead, the potentials seek those levels required to satisfy the integrated current condition imposed together with the equilibrium potentials and the polarization properties (including both electron-transfer and mass-transfer polarization components) of the one or more redox reactions that can take place. The model predicts actual values of the potentials at the emitter surface as a function of location, as well as the amount of current supplied by each of the different redox reactions. In previous ES-MS and ES-PDA work, the maximum value of the emitter interface potential and the current distribution among the different reactions could only be inferred on the basis of the redox reaction products observed in the respective spectra. Obviously, a next step towards validating the model must involve simulating a system in which the products of two or more redox reactions that may take place can each be observed in the gas-phase by ES-MS. The ES-MS signal intensity of each of these electrochemically generated ions should reflect their respective solution concentrations as they exit the emitter. For example, a mixture of two or more different metallocenes[31] or metalloporphyrins[32], each having very similar structure (and therefore similiar ES-MS signal response), but different equilibrium potentials and other documented electrochemical parameters might serve as a good test case. With such a system the predicted solution concentration of each

reaction product may be compared with the gas-phase ion abundances observed in an actual ES-MS experiment. One the basis of such results, the model may be more fully evaluated and altered as necessary.

The second piece of important information derived from this modeling regards the effective electrode area within the ES emitter. Although the total length of the inner surface of the emitter modeled (1 mm in length) was in contact with the electrolyte, the majority of the current owing to the redox reactions originated within a 200-300 μm region near the spray tip. This limited effective anode area, equal in length to approximately three emitter inner diameters or less, is a direct consequence of the limited penetration of the electric field into this high-aspect-ratio geometry. The current density distribution must follow the limitations of this potential gradient distribution. This has direct consequences for "nano-ES" [33] devices where the emitter diameter is much smaller (on the order of a few micrometers). Although the effective electrode length determined in the current simulations is small relative to the total emitter length, this effective electrode length is large relative to that provided, for example, in a metal coated, glass nano-ES capillary. For a typical nano-ES emitter inner diameter of 10 μm, the physical limit to the electrode length is probably only a few micrometers at most. This is because metal contact with the solution is made only at the outer rim of the emitter at the spray tip. Because nano-ES emitters as currently operated generate nearly the same absolute currents as ES emitters of conventional size, but at the same time are geometrically much smaller, the local current densities at the metal contact in a nano-ES emitter will be increased much above those found in the present calculations. This will substantially alter the polarization, and may in the extreme result in a different interfacial charge transfer mechanism. Since the polarization is in any event a highly nonlinear process, it may be difficult to accurately extrapolate from these 100-μm tube diameters to very small devices (1-10 μm), unless new ways of controlling current are utilized. Even if the charge transfer mechanisms do not change, if higher current densities and thus higher overpotentials are used, there will be a trend toward less selectivity for reactions. It is possible, though, that use of smaller diameters will permit reacting higher percentages of analyte. Further simulations on this scale would be needed to answer these

questions. Such simulations could guide the optimization of emitter diameter, flow rate, current-control schemes, and choices of redox buffers.

There are other questions involving changes in electrode configuration up to and including the possibility of through-glass conduction in glass nano-ES capillaries, and also involving the behavior of the region in space between the Taylor cone and the counter-electrode plate. These issues would require introducing functional relationships for different and as yet poorly-understood phenomena.

In addition to the simulation/ES-MS comparison study mentioned above, additional studies are planned to refine and expand our modeling capabilities. In its current form, the model neglects the possibility of depletion of the bulk concentration of a reacting species. This will be altered so that a more true reflection of current distributions of individual analyte reactions may be obtained. Also, we will attempt to model more than two redox reactions within the emitter, including emitter corrosion. This latter reaction contributes metal ions to solution that may contribute to chemical noise in the ES mass spectrum.[3,17] Also, this reaction ultimately leads to the need to periodically replace the commonly used stainless steel ES emitter to maintain optimum performance in ES-MS. We also will want to model different ES emitter geometries used in ES-MS. The other most common alternative arrangement to that modeled here is a grounded metal emitter with a counter electrode held at high voltage. Nano-ES configurations include a metal-coated pulled capillary, and pulled capillaries where high voltage or ground contact to solution is made upstream via a metal connector, wire, or other conductive contact.

The results from these simulations will facilitate our ability, through knowledge of the proper ES operational parameters and geometry, to promote or inhibit certain redox reactions to analytical advantage in the context of ES-MS. Among the benefits of such control are the ability to promote electrochemical ionization of analytes for enhanced ES-MS detection, to create novel ionic species in ES-MS (e.g., $M^{+\cdot}$, M^{2+} versus $(M+H)^+$, $(M+2H)^{2+}$, and to study analyte redox chemistry[5]. The latter case relates to the possible use of ES-MS as a new tool for electrochemical studies. Close coupling of ion generation with MS ion detection offers, for example, an alternative to the rotating ring-disk electrode commonly used for mechanistic studies.

The CCE-cell-like behavior of this system indicates that redox buffers, chosen judiciously so as not to affect the gas-phase ion generation process, might be used to maintain the interface potentials within the emitter to within specified limits. In this way, the redox products for a given analyte that might be observed in the ES mass spectra are assured of being formed from reactions that took place at or below the potential maintained by means of the redox buffer. The amounts of material needed for such investigation (pmol levels) are much smaller than needed for many traditional electrochemical studies and analysis of reaction products is immediate. The ability to inhibit unwanted reactions might also be of analytical advantage. The ability to avoid unwanted analyte electrolysis reactions avoids confusion in the analysis of unknowns that might be chemically altered by such reactions[5]. Also, this may avoid a possibly undesirable distribution of charge among different ionic species. Furthermore, control of the reactions would allow one to control changes in bulk solution composition such as pH that might result from the redox reactions.[16]

APPENDIX

Determination of the Size of the Virtual Cathode. In the electrospray process the Taylor cone ejects a jet from its vertex which, during the transit away from the vertex, breaks up into droplets. The radial (lateral) surface of the cone is an insulated surface, and thus the flow of ions from the anode out of the system is constrained to flow into the base of the jet. The fluid leaves the region of the cone vertex and breaks down into droplets, taking the ions along. We have assumed the simple mode of jet operation, leading to a single-thread jet ejected from the cone frustum. So, the base of the jet represents an area through which all of the ions must flow. The effects of subsequent mechanisms operating in the inter-electrode space that affect the flow of ions in the jet, droplets and beyond, are assumed to be somewhat isolated from the electrolyte within the emitter. We have assumed that all external effects influence the interior electrolytic phenomena only by modifying the voltage of the virtual cathode. The size of the virtual cathode was determined from estimates of the jet and droplet size for the system under investigation.

The jet radius is calculated from expressions of Kebarle and Ho.[33] First we calculate the electric field in the gas space at the tip of the Taylor cone, E_c,

$$E_c = \frac{2V_a}{R_c \ln\left(4\frac{d}{R_c}\right)}$$

where: V_a = applied voltage, 3500V; R_c = capillary outer radius, 200×10^{-6} m; and d = distance from capillary to counter electrode, 0.01 m.

This value of the electric field is used to calculate the radius of the droplet, using

$$r_d = \left(\frac{3\varepsilon\gamma^{\frac{1}{2}}U}{4\pi\varepsilon_0^{\frac{1}{2}}KE_c}\right)^{\frac{2}{7}}$$

where: ε = permittivity, 36.25 ε_0, Farad/m; γ = Surface tension, 29.02×10^{-3} N/m; K = conductivity of liquid, 3.8×10^{-6} Mho/m; and ε_0 = permittivity of vacuum, 8.854×10^{-12}, Farad/m.

Kebarle and Ho[33] report that this expression matches with experimental data and agrees with other semi-empirical expressions, but it was developed using assumptions that are unproven.

The radius of the jet is obtained by

$$r_j = \frac{r_d}{1.9}$$

where r_d is the radius of drops resulting from the breakup of the ejected jets of radius r_j. Thus the virtual cathode would be of radius r_j.

These data for the CH_3CN/H_2O (90/10 v/v) system under the specified experimental conditions produce a calculated jet radius of 4.1 μm, which was used in the model of the interior electrolyte system. Although other estimates of the emission radius produce different estimates of the jet base (see for example Wilm and Mann[34]) these values are similar in order-of-magnitude. The virtual cathode is separated from the anode by a distance of 58 μm and thus the exact value of the

virtual cathode size should not have a large influence on the nature of the oxidation of the analyte on the anode, given that the angle of the Taylor cone is fixed at 49.3°.

ACKNOWLEDGEMENTS

Research was sponsored by the Division of Chemical Sciences, Office of Basic Energy Sciences, by the Applied Mathematical Sciences Research Program of the Office of Mathematical, Information, and Computational Sciences, both under contract DE-AC05-96OR22464 with Oak Ridge National Laboratory, managed by Lockheed Martin Energy Research Corporation; and by Defense Programs of the Department of Energy, under contract DE-AC05-84OR21400 with the Oak Ridge Y-12 Plant, managed by Lockheed Martin Energy Systems, Inc.

REFERENCES

(1) *Electrospray Ionization Mass Spectrometry*, Cole, R.B., Ed., John Wiley: New York, 1997.

(2) Gaskell, S. J. *J. Mass Spectrom.*, **1997**, *32*, 677-688.

(3) Blades, A. T.; Ikonomou, M. G.; Kebarle, P. *Anal. Chem.* , **1991**, *63*, 2109-2114.

(4) Van Berkel, G. J.; Zhou, F. *Anal. Chem.* , **1995**, *67*, 2916-2923.

(5) Van Berkel, G. J. Chapter 2 in *Electrospray Ionization Mass Spectrometry*, Cole, R.B., Ed., John Wiley: New York, 1997, pp. 65-105.

(6) Tang, L.; Kebarle, K. *Anal. Chem.* , **1991**, *63*, 2709-2715.

(7) Enke, C. G. *Anal. Chem.* , **1997**, *69*, 4885-4893.

(8) Ikonomou, M. G.; Blades, A. T.; Kebarle, P. *Anal. Chem.* , **1991**, *63*, 1989-1998.

(9) Charbonnier, F.; Rolando, C.; Saru, F.; Hapiot, P.; Pinson, J., *Rapid Commun Mass Spectrom.*, , **1993**, *7*, 707-710.

(10) *Electroanalytical Measurements in Flowing Liquids*; Ellis Horwood: Stulik, K.; Pac<kov<, V. , Chichester, West Sussex, England, 1987.

(11) *Laboratory Techniques in Electroanalytical Chemistry*, Kissinger, P. T.; Heineman, W. R., Eds.; Marcel Dekker: NewYork, 1996.

(12) Pfeifer, R. J.; Hendricks, C. D. *AIAA J.* , **1968**, *6*, 496-502.

(13) Juhasz, P.; Ikonomou, M. G.; Blades, A. T.; Kebarle, P, "Electrospray, Mechanism and Performance", in *Methods and Mechanism for Producing Ions from Large Molecules*, edited by K. G. Standing and W. Ens, Plenum Press, New York, 1991, pp 171-184.

(14) Kebarle, P.; Tang, L. *Anal. Chem.* , **1993**, *65*, 972A-986A.

(15) Van Berkel, G. J.; Zhou, F. *J. Am. Soc. Mass Spectrom.* ,**1996**, *7*, 157-162.

(16) Van Berkel, G. J.; Zhou, F.; Aronson, J. T. *Int. J. Mass Spectrom. Ion Processes,* **1997**, *162*, 55-67.

(17) Van Berkel, G. J. *J. Anal. At. Spectrom.*, **1998**, *13*, 603-607.

(18) Van Berkel, G. J.; Zhou, F. Anal. Chem., **1995**, *67*, 3958-3964.

(19) Van Berkel, G. J.; Quirke, J. M. E.; Tigani, R. A.; Dilley, A. S.; Covey, T. R. *Anal. Chem.* , **1998**, *70*, 1544-1554.

(20) Giles, G. E.; Gray, L. J.; Bullock, J. S., IV *BEPLATE - Simulation of Electrochemical Plating*, K/CSD/TM-89, Martin Marietta, September 1990.

(21) Brebbia, J. C.; Telles, F.; Wrobel, L. C. *Boundary Element Techniques*, Springer Verlag, Berlin and New York (1984).

(22) L. J. Gray, *A Program for Solving the 3-Dimensional Laplace Equation via the Boundary Element Method*, ORNL/TM-9816, Martin Marietta Energy Systems, Inc., Oak Ridge National Laboratory, Oak Ridge, Tennessee, 1986.

(23) Newman, J. S. *Electrochemical Systems*, Second Edition, Prentice Hall, Englewood, NJ, 1991.

(24) Hoare, J. P. The Electrochemistry of Oxygen, Interscience, New York, 1968

(25) Kuwana, T.; Bublitz, D. E.; Hoh, G., *J. Am. Chem. Soc.* , **1960**, *82*, 5811-5817.

(26) The Encyclopedia of Electrochemistry , C. A. Hampel, Ed., Reinhold, New York, 1964.

(27) Bockris, J. O'M.; and Reddy, A. K. N.; Modern Electrochemistry, vol. 2., Plenum Press, New York, 1970.

(28) Janz, G. J.;and Tomkins, R. P. T.; Nonaqueous Electrolytes Handbook, vol. 1, p. 85, Academic Press, New York and London, 1972.

(29) Hayati, I.; Bailey, A.; Tadros, Th. F., Nature, **1986**, *319*, 41-43.

(30) Korn, G. A.; and Korn, T. M.; Mathematical Handbook for Scientist and Engineers, Second Edition, McGraw-Hill, New York, 1968, sect 9.2-5.

(31) Xu, X.; Nolan, S. P.; Cole, R. B. *Anal. Chem.*, **1994**, *66*, 119-125

(32) Vandell, V. E.; Limbach, P. A. *J. Mass Spectrom.*, **1998**, *33*, 212-220.

(33) Wilm, M. S.; Mann, M., Int. J. Mass Spectrom. Ion Processes, **1994**, *136*, 167-180.

(34) Kebarle, P.; Ho, Y., Chapter 1 in Electrospray Ionization Mass Spectrometry, Cole, R. B., ed., John Wiley : New York, 1997.

FIGURE HEADINGS

Figure 1. (a) Geometry of ES system modeled showing the metal emitter capillary (i.e, the working electrode) positioned normal to the aperture plate (i.e., counter electrode) of the mass spectrometer and held at a high positive voltage relative to this counter electrode. (b) Longitudinal cross section of the emitter near the spray tip showing the solution flowing through the emitter and the truncated Taylor cone, the frustum of which is treated as a virtual cathode in the ES model.

Figure 2. Schematic representation of multiple reaction polarization technique showing current pathways and relative potentials. Voltage differences are not drawn to scale.

Figure 3. Structures and processes at different dimensional scales within the ES emitter tip. Hydrodynamic boundary layer for fully developed momentum boundary layer extends to the centerline of the tube. X equals Y for fully developed concentration boundary layer. OHP = outer Helmholtz plane, IHP = inner Helmholtz plane.

Figure 4. (a) Calculated current densities for H_2O oxidation (thin solid line), ferrocene oxidation (thin dotted line), total current density (thick solid line), and the calculated interface potentials, V_{0A} (dot dash line), each plotted as a function of axial position from the tip (0 μm) to 1000 μm upstream into the emitter. (b) Same data as in (a) plotted to show details of the region 250 μm from the spray tip. Modeling conditions: CH_3CN/H_2O (90/10 v/v) with 5.0 μM Fc, conductivity = 3.8×10^{-7} Mho/cm, ES current = 5.21×10^{-8} A. Other electrochemical parameters as shown in Table 1.

Figure 5. Data from Figure 4 plotted as log(current density) versus interface potential, V_{0A}, H_2O oxidation current density (thin solid line), Fc oxidation current density (thin dotted line), and total current density (thick solid line).

Figure 6. Plots of (a) interface potential, V_{0A}, versus axial position within the ES emitter and (b) the integrated fraction of the total ES current owing to H_2O oxidation (dotted lines) and Fc oxidation (solid lines) for [Fc] = 5 (■), 10 (◆), 20 (●), and 50 (▼) μM. Modeling conditions: CH_3CN/H_2O (90/10 v/v), conductivity = 3.8×10^{-7} Mho/cm, ES current = 5.21×10^{-8} A. Other electrochemical parameters as shown in Table 1.

Figure 7. Plots of (a) interface potential, V_{0A}, versus axial position within the ES emitter and (b) the integrated fraction of the total current owing to H_2O oxidation (dotted lines) and Fc oxidation (solid lines) for solution conductivities of 1.9 (▼), 3.8 (■) and 7.6 (▲) $\times 10^{-7}$ Mho/cm. Modeling conditions: CH_3CN/H_2O (90/10 v/v), 5.0 μM Fc, ES current = 5.21×10^{-8} A. Other electrochemical parameters as shown in Table 1.

Table 1. Electrochemical Parameters used for Calculation of Ferrocene and H_2O Oxidation in the ES Emitter for a CH_3CN/H_2O (90/10 v/v) Solution Containing 5.0 μM Ferrocene.

parameter	units	H_2O oxidation (eq 11)	Fc oxidation (eq 12)
α_A		0.493	0.493
I_{0A}	(A/cm^2)	1×10^{-12}	5×10^{-10}
E_{0A}	(V vs SHE)	1.229	0.572
I_l	(A/cm^2)	1×10^{-3}	4.82×10^{-5}
D	(cm^2/s)	1×10^{-5}	2.4×10^{-5}

Table 2. Fc oxidation as a function of concentration

[Fc] (μM)	Fc flux through emitter[a] (equiv/s)	Total ES current[b] (equiv/s)	Fc oxidation current[c] (c/s)	Fc oxidation current[c] (equiv/s)	% Fc oxidized
5	4.17×10^{-13}	5.39×10^{-13}	4.43×10^{-9}	4.59×10^{-14}	11.0
10	8.33×10^{-13}	5.39×10^{-13}	6.79×10^{-9}	7.04×10^{-14}	8.45
20	1.67×10^{-12}	5.39×10^{-13}	1.05×10^{-8}	1.09×10^{-13}	6.53
50	4.17×10^{-12}	5.39×10^{-13}	1.84×10^{-8}	1.91×10^{-13}	4.58

[a] Fc flux = [Fc]×flow rate/n where n = 1

[b] Integration of local currents calculated in BEPLATE™ model

for all cases = 5.21×10^{-8} c/s (5.39×10^{-13} equiv/s)

[c] Integration of the local Fc oxidation currents in model

Table 3 Fc oxidation as a function of conductivity

[Fc]	Conductivity	Total ES	Total ES	Fc oxidation	Fc oxidation	% Fc

(μM)	Mho/cm^2	current[b] (c/s)	current[b] (equiv/s)	current[c] (c/s)	current[c] (equiv/s)	oxidized
5	7.6×10^{-7}	1.04×10^{-7}	1.11×10^{-12}	5.86×10^{-9}	6.07×10^{-14}	14.6
5	3.8×10^{-7}	5.21×10^{-8}	5.40×10^{-13}	4.43×10^{-9}	4.59×10^{-14}	11.0
5	1.9×10^{-7}	2.61×10^{-8}	2.70×10^{-13}	3.36×10^{-9}	3.48×10^{-14}	8.35

a,b, and c as in Table 2. For all cases in this table flow rate = 5 μl/min

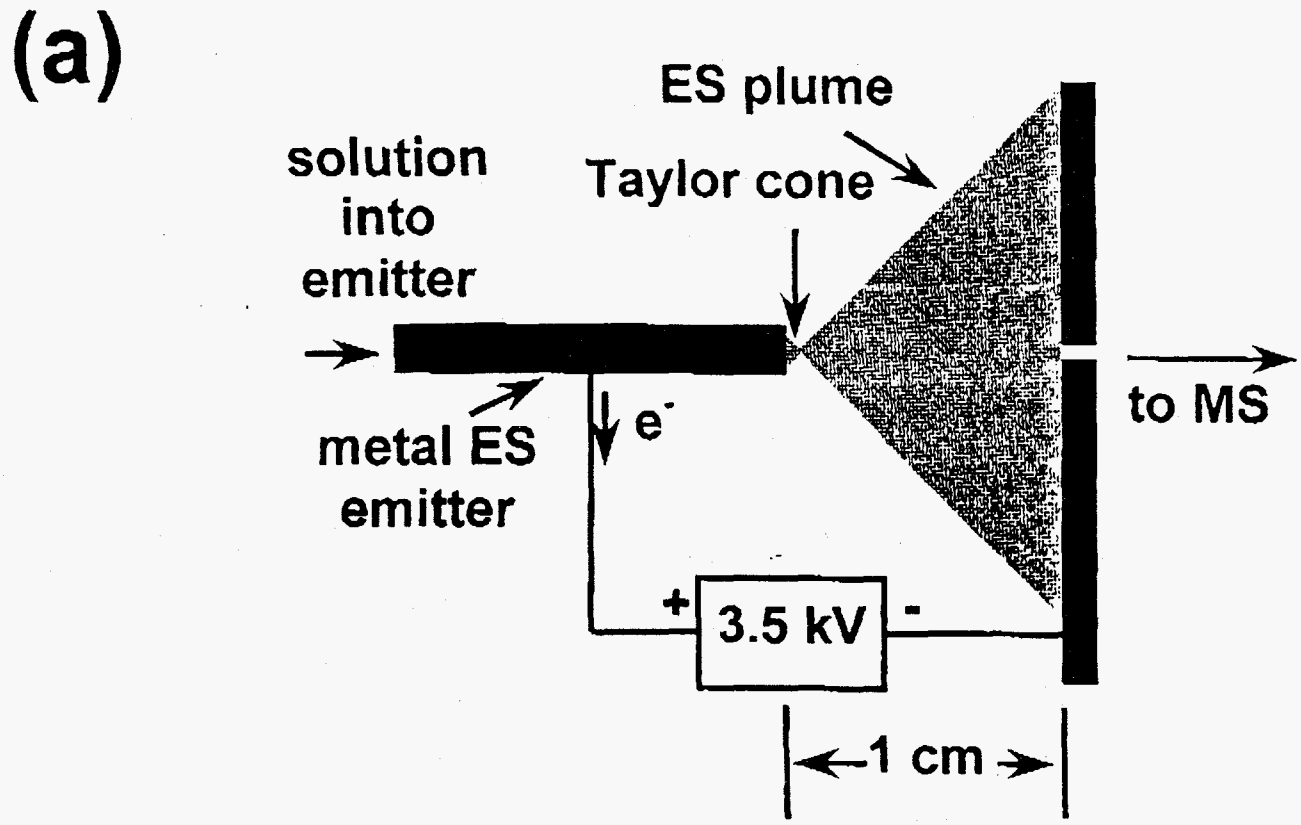
(a)
ES plume
Taylor cone
solution into emitter
to MS
metal ES emitter
e-
+
3.5 kV
-
1 cm

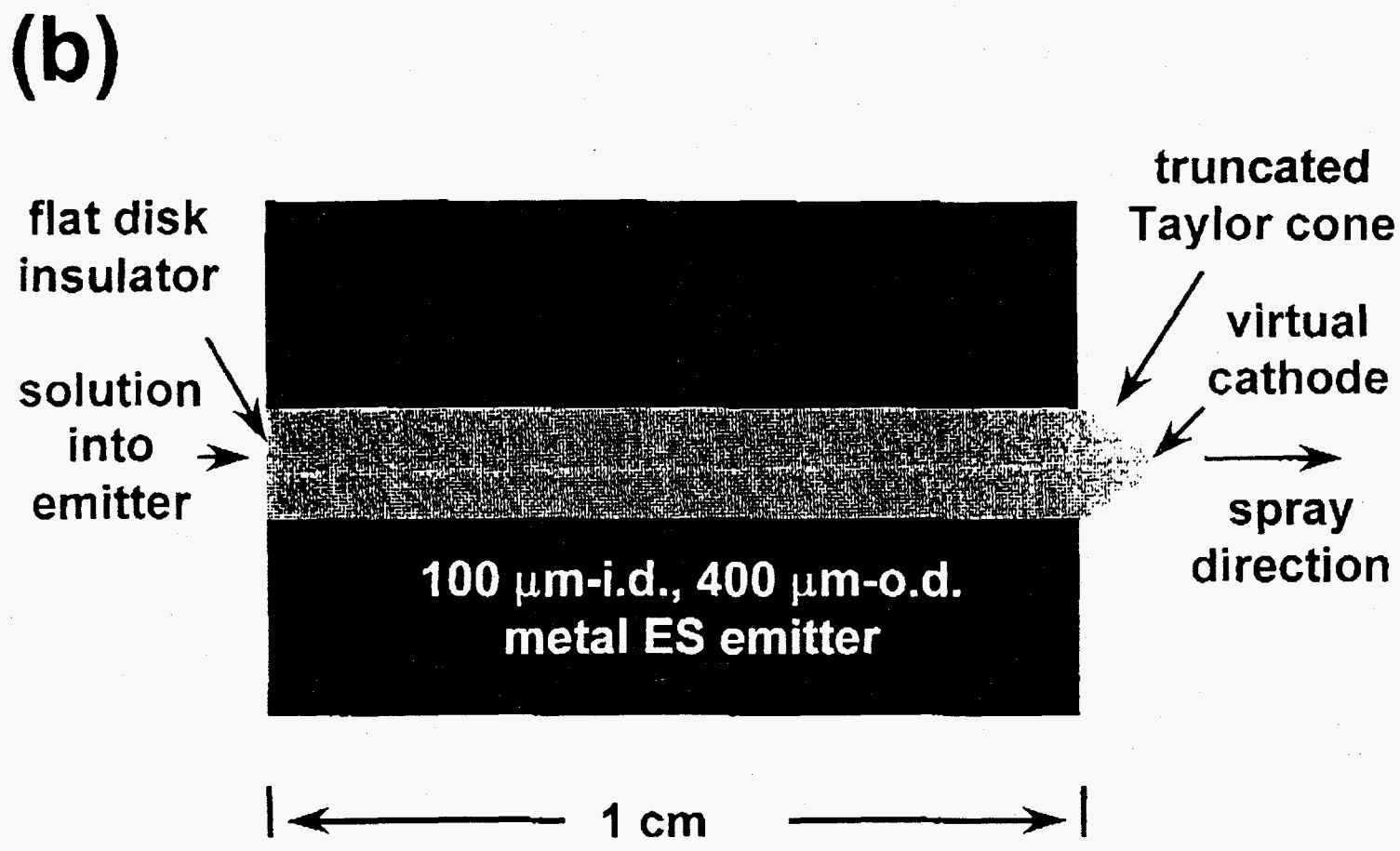
(b)
truncated Taylor cone
flat disk insulator
virtual cathode
solution into emitter
spray direction
100 μm-i.d., 400 μm-o.d.
metal ES emitter
1 cm

Figure 1 –

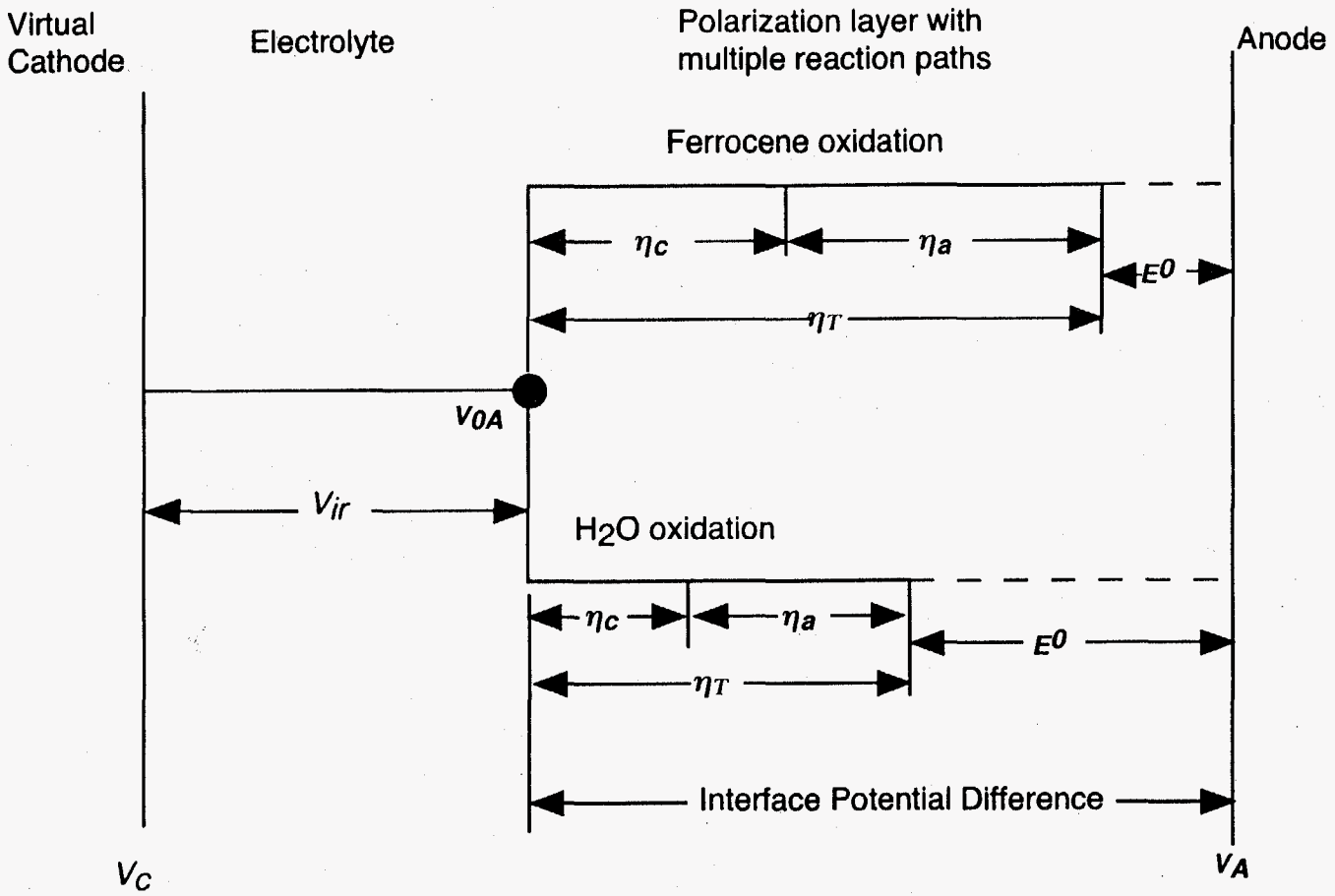

Voltage differences are not to scale

Fig. 2 - Multiple Reaction Paths

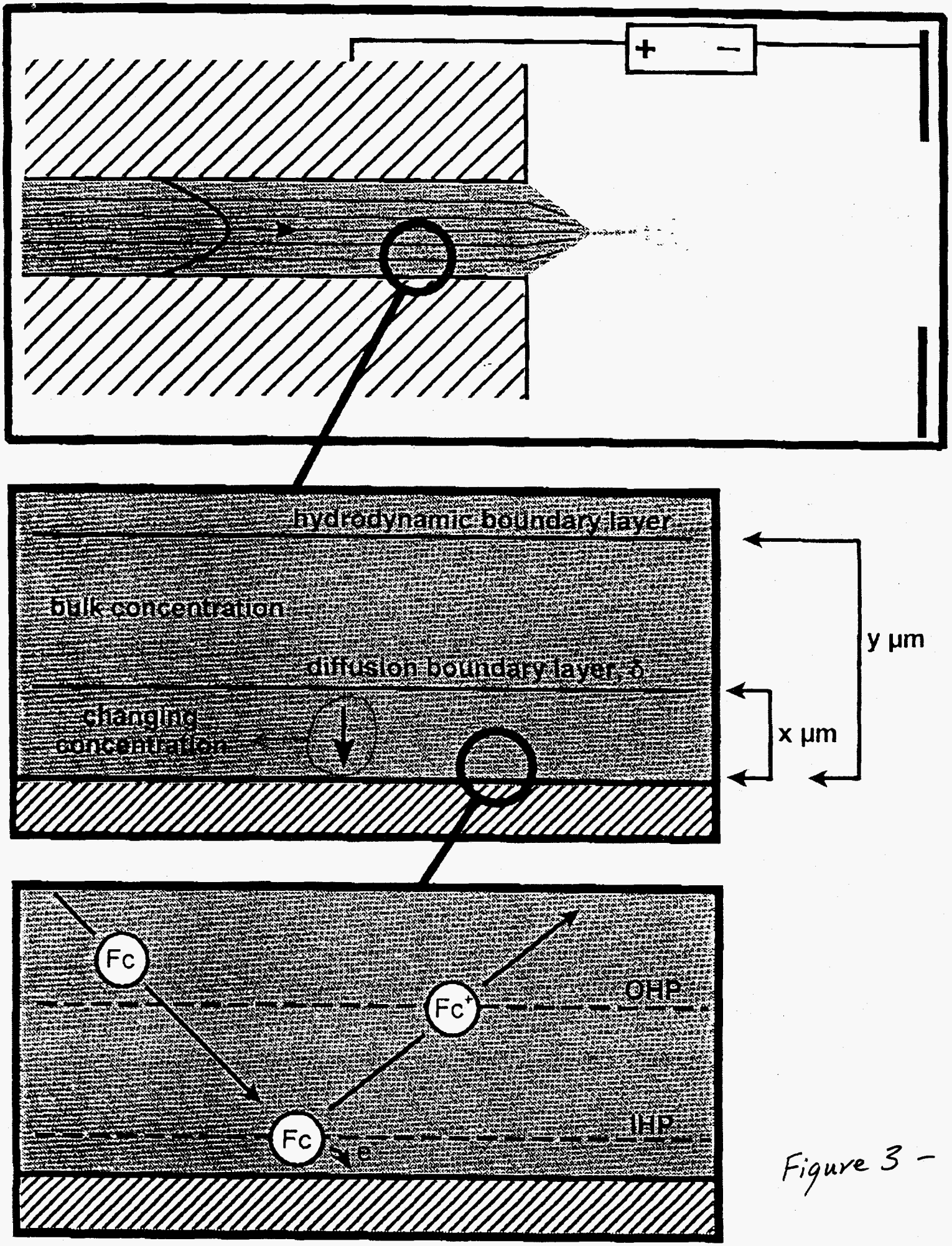
+
−
hydrodynamic boundary layer
bulk concentration
diffusion boundary layer, δ
changing concentration
y µm
x µm
Fc
Fc+
OHP
IHP
e

Figure 3 -

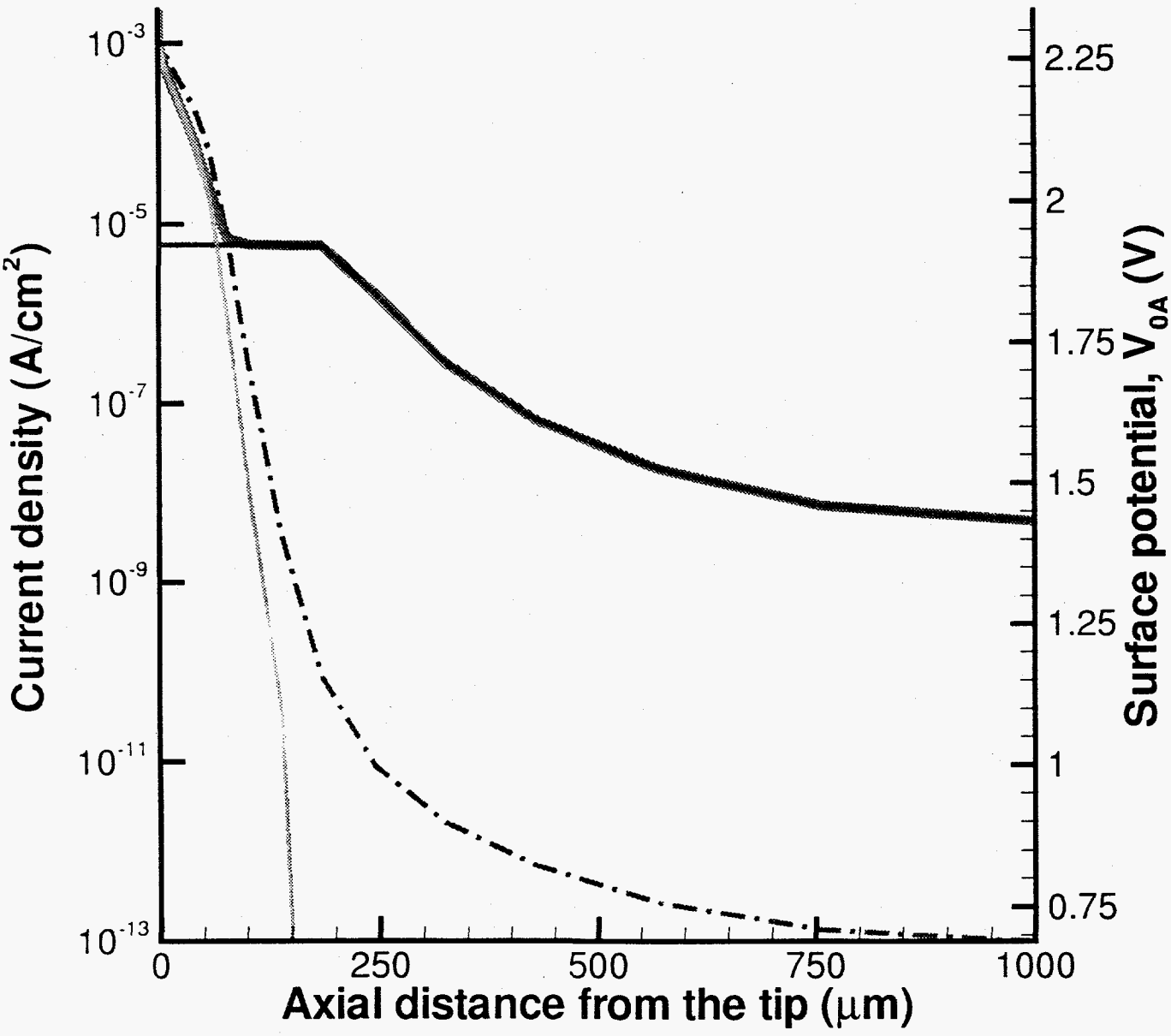
Current density (A/cm^2)
10^{-3}
10^{-5}
10^{-7}
10^{-9}
10^{-11}
10^{-13}
Surface potential, V_{0A} (V)
2.25
2
1.75
1.5
1.25
1
0.75
0
250
500
750
1000
Axial distance from the tip (μm)

Figure 4a -

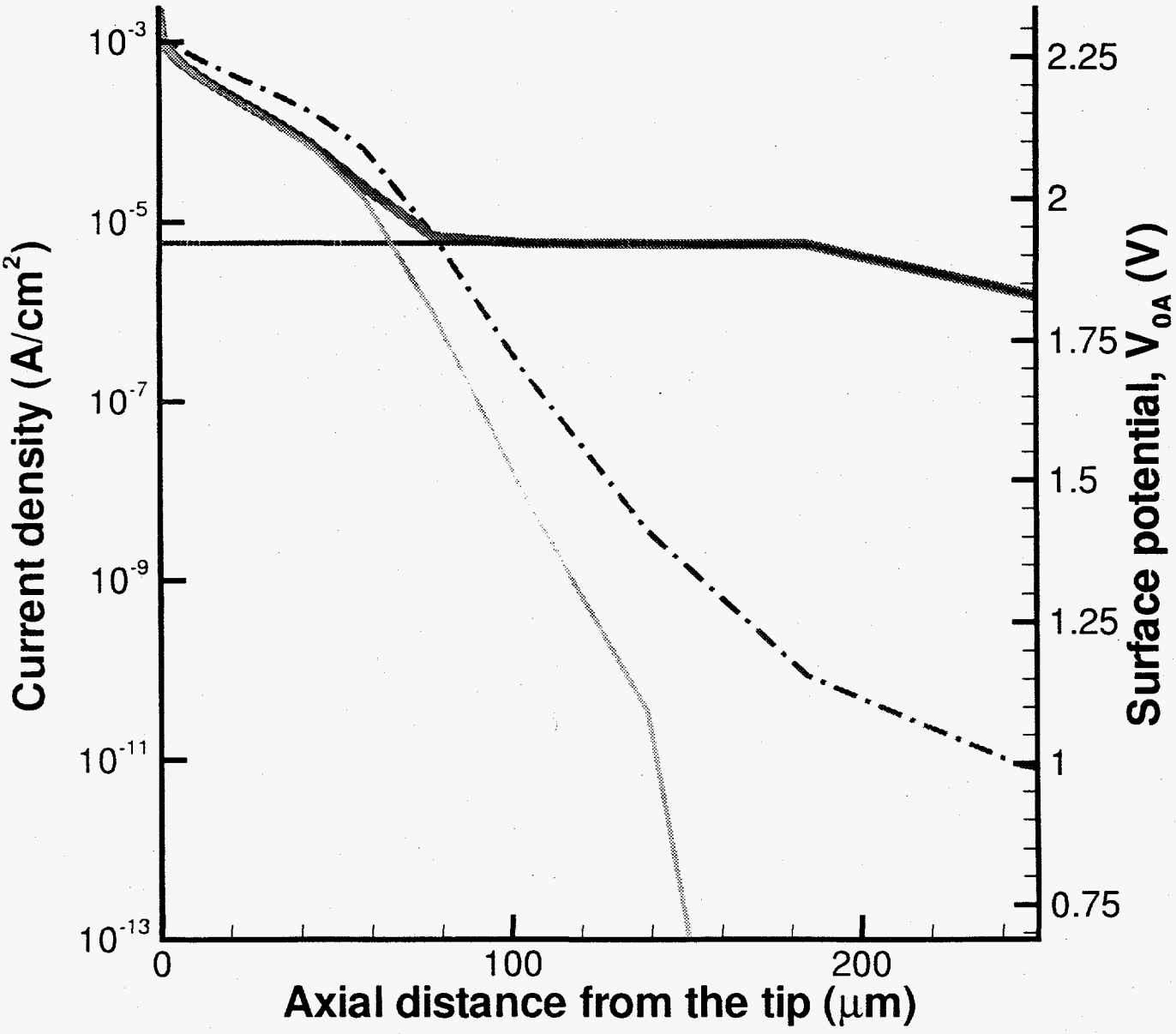
Current density (A/cm^2)
10^{-3}
10^{-5}
10^{-7}
10^{-9}
10^{-11}
10^{-13}
Surface potential, V_{0A} (V)
2.25
2
1.75
1.5
1.25
1
0.75
0
100
200
Axial distance from the tip (μm)

Figure 4 b –

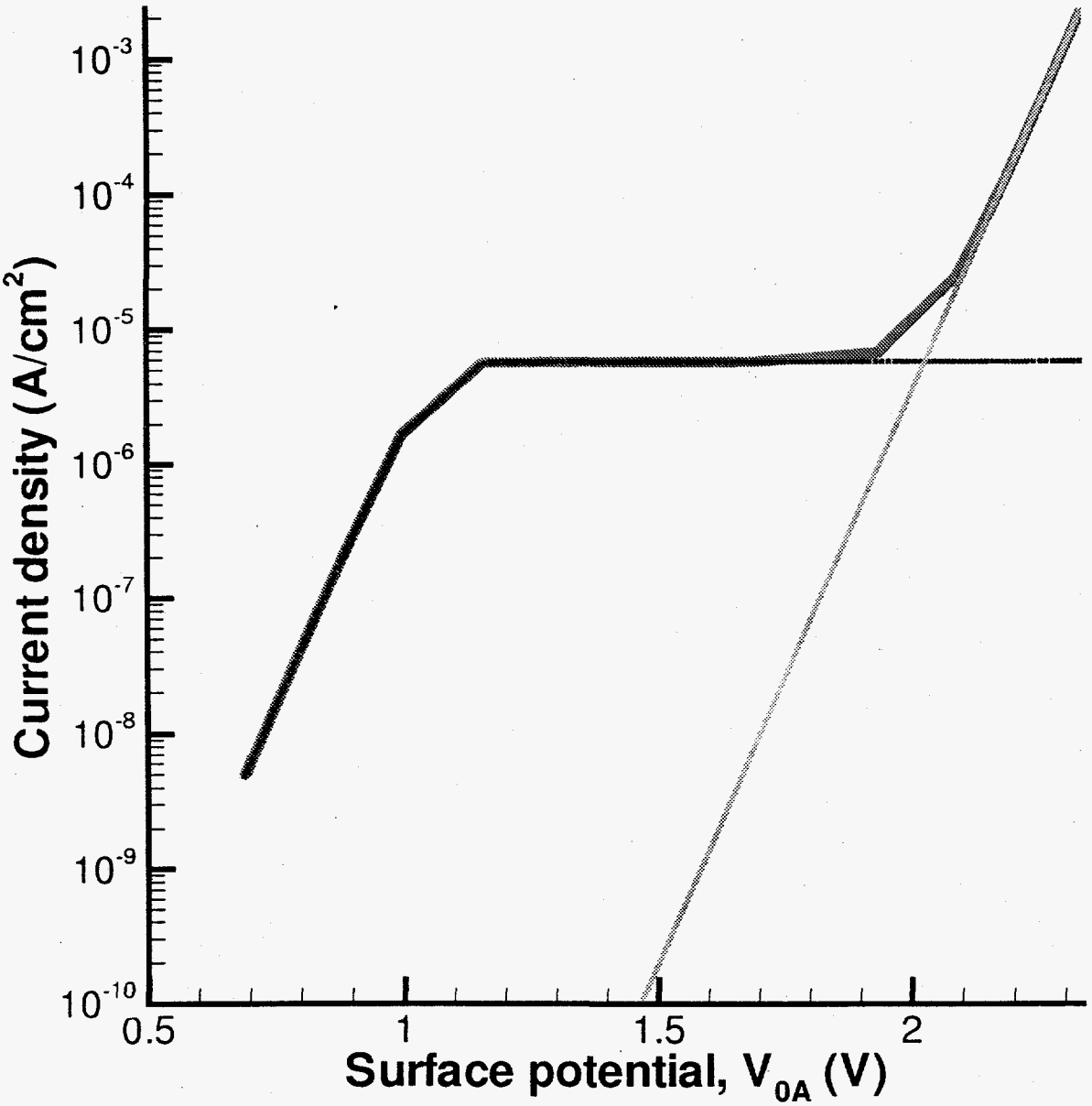
Current density (A/cm^2)
10^{-3}
10^{-4}
10^{-5}
10^{-6}
10^{-7}
10^{-8}
10^{-9}
10^{-10}
0.5
1
1.5
2
Surface potential, V_{0A} (V)

Figure 5 -

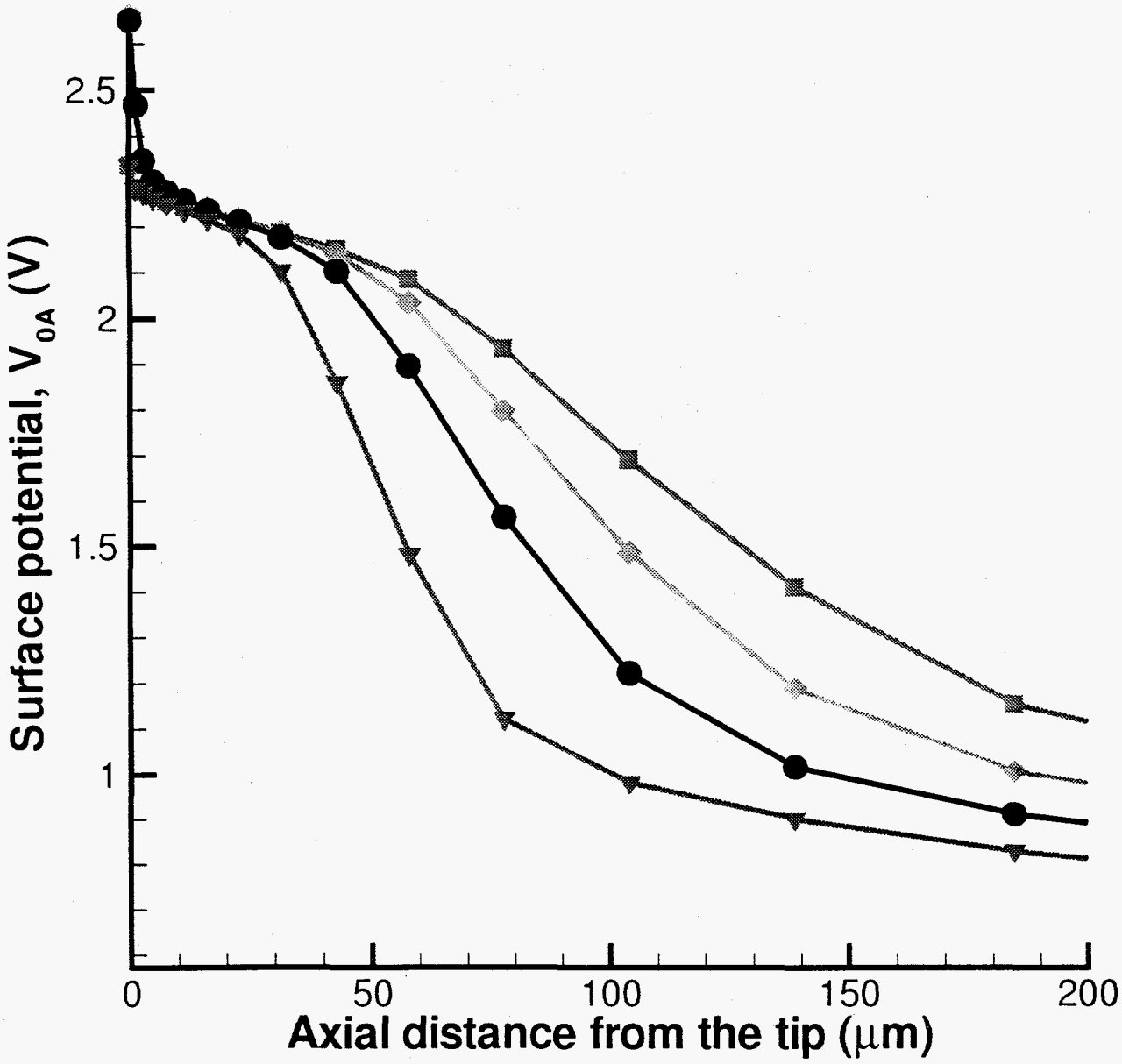
Surface potential, V_{0A} (V)
2.5
2
1.5
1
0
50
100
150
200
Axial distance from the tip (μm)

Figure 6a –

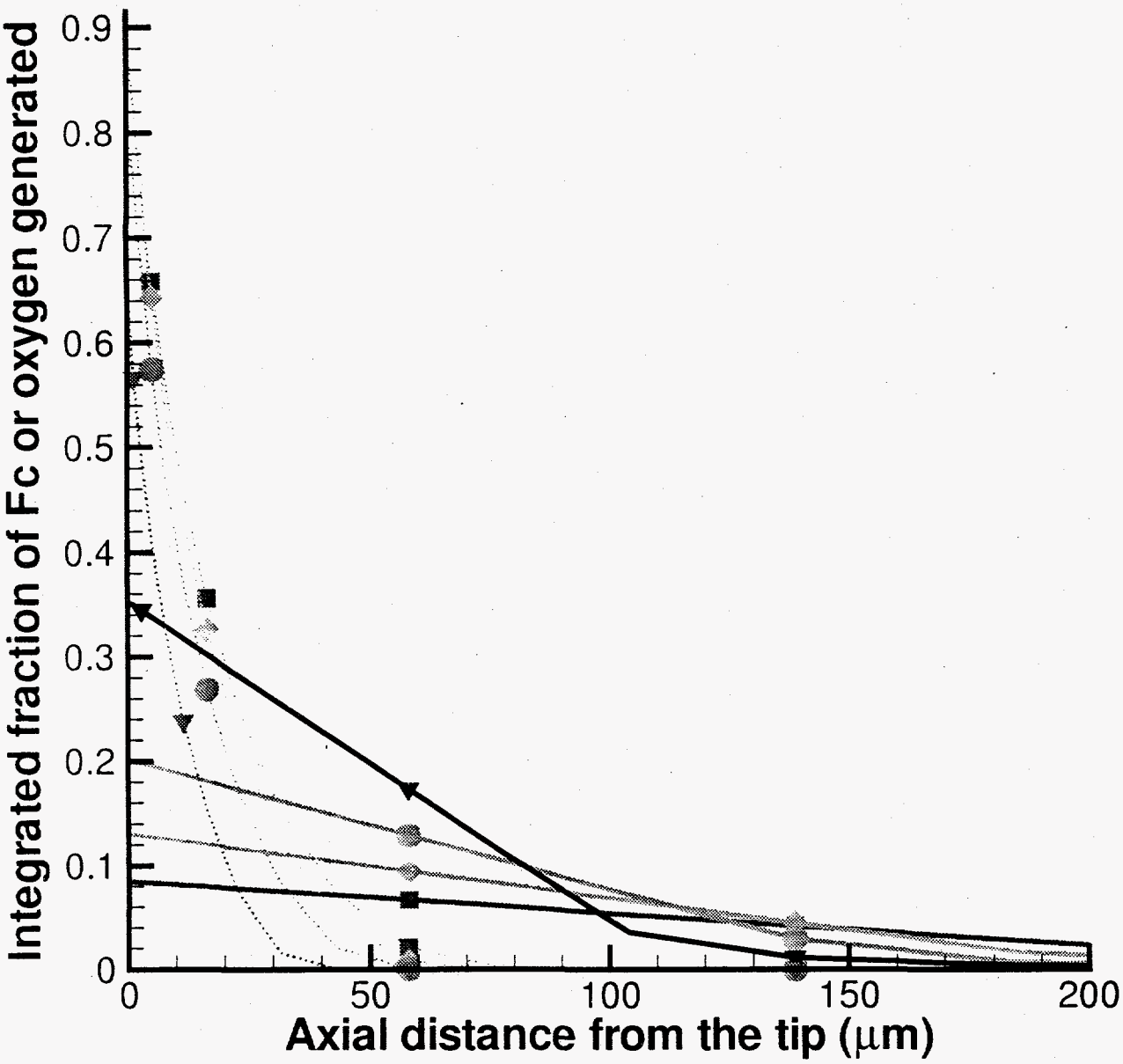
Integrated fraction of Fc or oxygen generated
0.9
0.8
0.7
0.6
0.5
0.4
0.3
0.2
0.1
0
0
50
100
150
200
Axial distance from the tip (μm)

Figure 6 b —

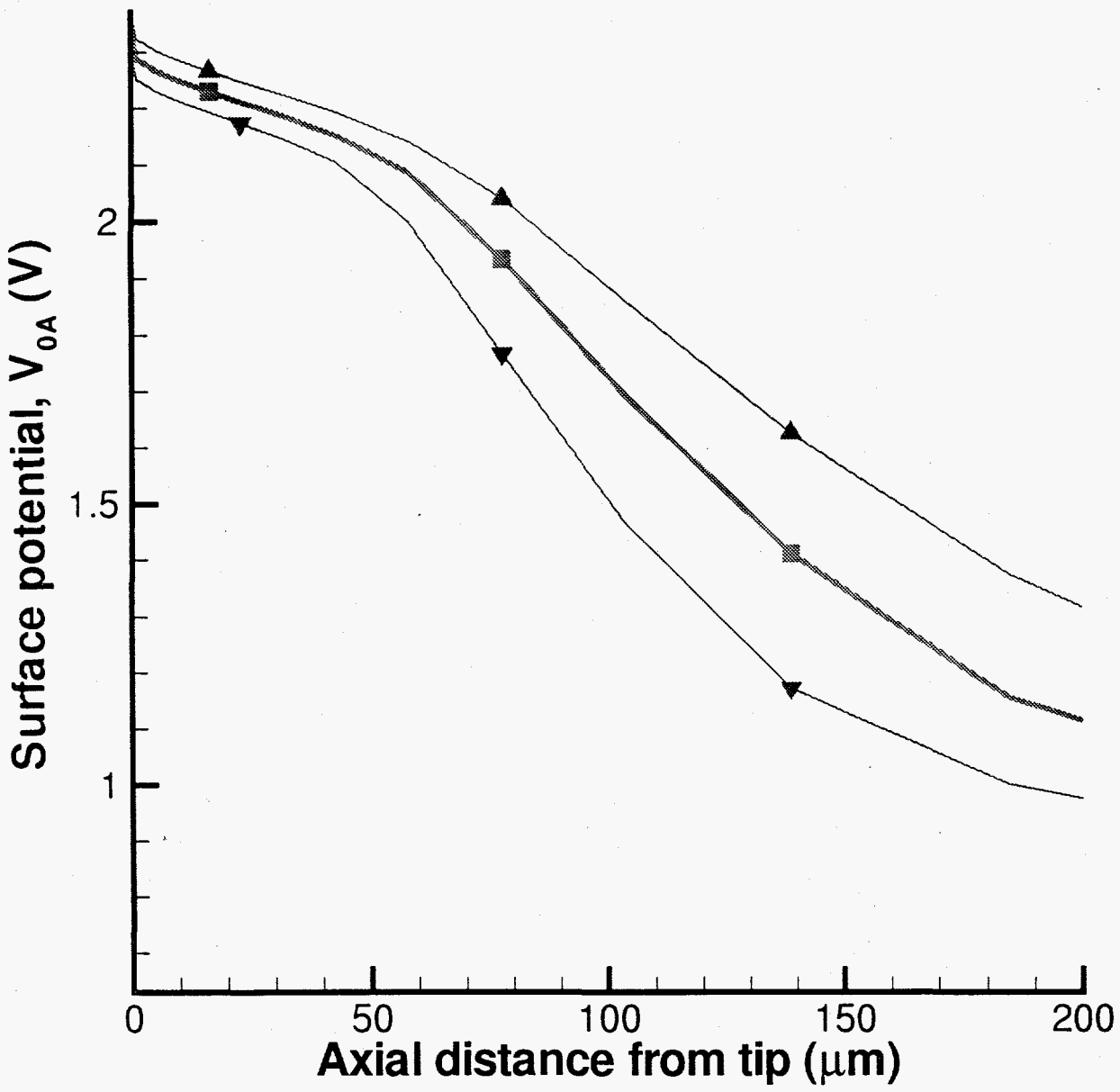
Surface potential, V_{0A} (V)
2
1.5
1
0
50
100
150
200
Axial distance from tip (μm)

Figure 7a –

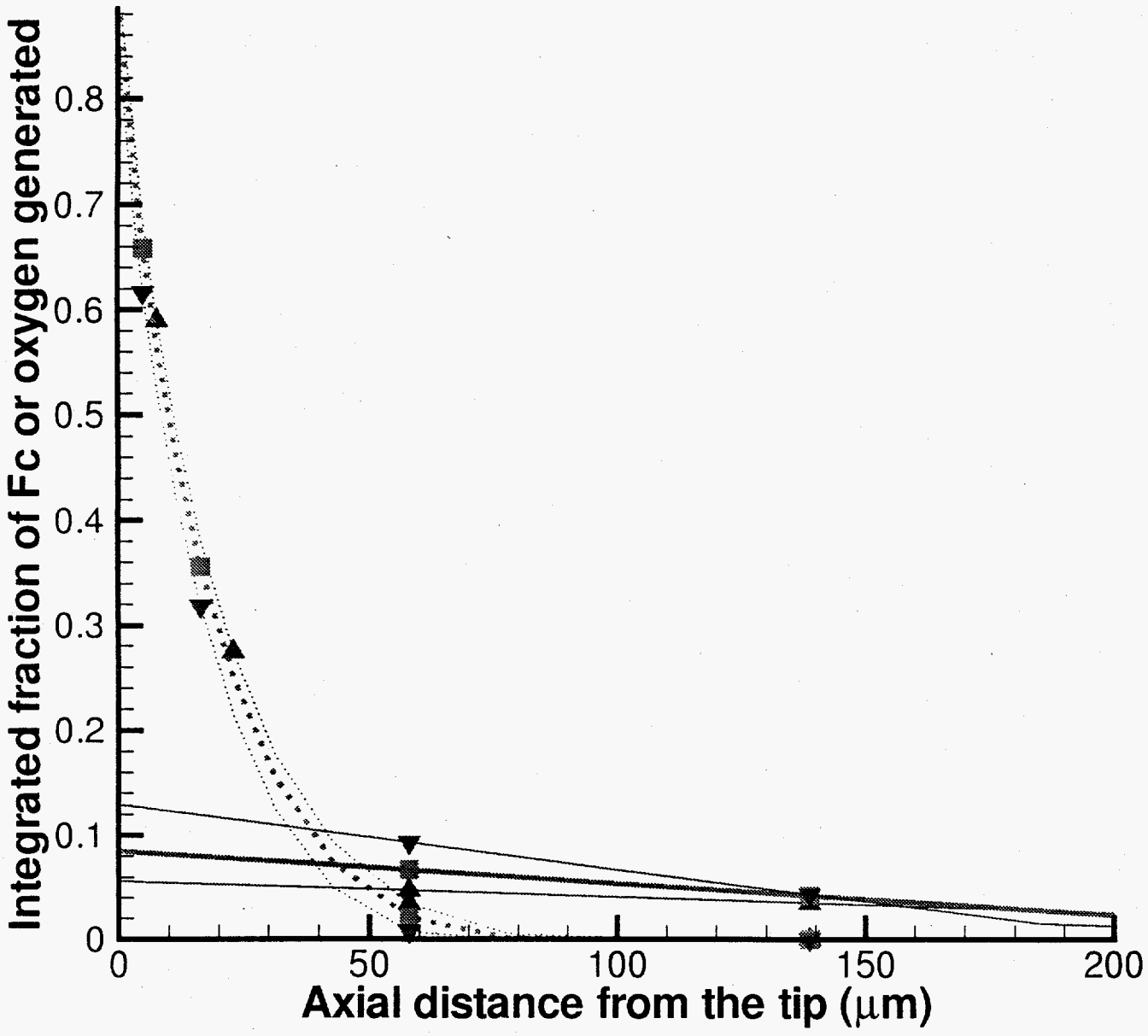
Integrated fraction of Fc or oxygen generated
0.8
0.7
0.6
0.5
0.4
0.3
0.2
0.1
0
0
50
100
150
200
Axial distance from the tip (μm)

Figure 7b —

Distribution:

J. S. Bullock
M. L. Baker/M. J. O'Hara
Plant Records (RC)

Distribution:

Recipients as designated by the author plus:

Y-12 Plant Records Services (3) 9711-5, MS-8169
[2 copies for OSTI and 1 copy for Central Files]

Note: This distribution page should not be included in the copy of your document (abstract, visuals, article etc.) submitted to a journal or technical society.